

Article

Coupled Multifield Response to Coordinate Mining of Coal and Uranium: A Case Study

Tong Zhang ^{1,2,3,*}, Liang Yuan ^{1,2,3}, Zhen Wei ^{1,2} and Yang Liu ¹

¹ State Key Laboratory of Mining Response and Disaster Prevention and Control in Deep Coal Mines, Anhui University of Science and Technology, Huainan 232001, China; 2018026@aust.edu.cn (L.Y.); 2018031@aust.edu.cn (Z.W.); 2017028@aust.edu.cn (Y.L.)

² School of Mining and Safety Engineering, An Hui University of Science & Technology, Huainan 232001, China

³ Beijing Key Laboratory for Precise Mining of Intergrown Energy and Resources, University of Mining and Technology (Beijing), Beijing 100083, China

* Correspondence: 2018013@aust.edu.cn

Received: 29 August 2019; Accepted: 30 November 2019; Published: 1 January 2020



Abstract: The coordinate mining of stack resources in the Ordos Basin, which involves the coupling effects of stress fracture, seepage, and reactive solute transport, plays an important role in resource exploration and environment protection. A coupled multiphysical–chemical model, involving a modified non-Darcy flow model, a leaching solution reaction, and a reactive solute transport model, was developed in this study. The Fast Lagrangian Analysis of Continua -Computational Fluid Dynamics (FLAC3D-CFD) simulator coupled with the developed models was used to investigate the evolution and morphology of mining-induced multifield coupling for the scenarios of concurrent mining and asynchronous mining of coal and uranium. As mining advanced to 160 m, the maximum principle stress characterized by a stress shell was observed. As mining progressed to 280 m, a rupture occurred, and a new stress shell was generated as a rear skewback was formed by the concentrated stress of the stope. An “arch-shaped” fracture field combined with a “saddle-shaped” seepage field was identified in the distressed zone of the stress shell. In the coordinated mining of uranium prior to coal, “funnel-shaped” and “asymmetric saddle-shaped” morphologies of the leaching solution were found during coal mining for ventilation in the stope and mining face. By contrast, “saddle-shaped”, “inclined funnel-shaped”, and “horizontal” morphologies of the leaching solution were observed for a short period for ventilation of the stope and mining face for coal mining prior to uranium mining, uranium mining prior to coal mining, and synchronized coal and uranium mining. A dynamic stress response was obtained in the coal seam, followed by the conglomerate aquifer and the uranium deposits. The diffusion depth of the solution was negatively correlated with the injection velocity and the pumping ratio and positively correlated with the diffusion coefficient. A dynamic increase in diffusion depth was observed as the diffusion coefficient increased to $1 \times 10^{-4} \text{ m}^2/\text{s}$.

Keywords: coordinated mining of coal and uranium; multiphysical–chemical model; FLAC3D-CFD simulator; multifield coupling

1. Introduction

With advanced mining equipment and technologies, longwall mining of coal seams [1–4] and in situ leaching of uranium [5–7] have been widely accepted. However, as a stack resource, the efficiency and safety of coal and uranium mining are important for energy demand, economic development, and ecological balance. Therefore, a new coordinated mining method has been proposed [8]. Coordinated mining, which involves physical mechanics and chemical reactions, is complex. It poses a threat to the

safety of underground water and the surface ecosystem [9,10]. In the past decades, considerable effort has been exerted to study geomechanical and geochemical responses to mining using methods that integrate theoretical analysis, simulation, and field measurements [11–13].

Substantial research on the hydromechanical effect on the mining layer has been conducted [14,15]. Wu et al. [16,17] and Liu et al. [18] proposed the strain–seepage, rheology–seepage, and variable parameter rheology–seepage models to deal with groundwater inrush problems under special geological conditions. Yang [19] developed a stress–damage–flow coupling model for groundwater outbursts and concluded that a dominant fracture developed in underlying overpressurized zones. Water pressure transmitted along open conduits reduced effective stresses and developed rapid heave displacements within the floor. Chen et al. [20] developed a coupled analysis model based on the Discontinuous Deformation Analysis (DDA) method and analyzed the fluid–solid coupling effect of a fractured rock. Kim et al. [21] proposed a finite, elastic, and porous model to study coupled rock deformation and groundwater flow from mining in saturated and fractured geological media. Xu et al. [22] investigated the influence of the main key stratum on the water-conducting height of a fractured zone and concluded that small and large water-conducting heights of the fracture zone were obtained for the mined geology, with large and small distances between the main key stratum and the coal seam. Xie et al. [23] discovered an arched stress shell located above the fracture field using numerical and physical simulation. They concluded that the stress shell bears the overburdened stress and transfers it into the skewback. Ma et al. [24], Li et al. [25], Dai et al. [26], and Chen et al. [27] investigated the development characteristics of a fractured zone and proposed corresponding preventive measures for the groundwater inrush of the stope.

In situ leaching of uranium involves the chemical reaction between the leaching solution and uranium, as well as the transport of a uranium-bearing solution in fractured porous media. The characteristics of the physical and chemical responses of mined deposits under different pumping ratios, pressure differences, and well spaces were extensively studied using an integrated method of experimentation and numerical simulation [28–30]. Simon et al. [31] conducted a batch test and column leaching experiment and then calibrated the reaction–transport parameters for in situ mining using the geochemical code CHES and the hydrodynamic geological code HYTEC. Dangelmayr et al. [32] studied the decay process of uranium under a certain hydraulic gradient via column leaching experimentation and the PHREEQC model. Gomez et al. [33] simulated uranium migration in underground water and obtained the reduction conditions of secondary uranium.

The coupled hydromechanical and hydrochemical mechanism and the distribution characteristics of mining-induced stress, fracture, fluid flow, and solute diffusion were studied and characterized. However, the hydrogeological response to the coordinate mining of coal and uranium, which utilizes the coupling effect of the stress–fracture–seepage field, solute chemical reaction, and transport and is crucial to safety and environment protection in mining, is rarely studied. Based on the stack occurrence of coal and uranium in the Ordos Basin, this study investigated the evolution and morphology of the stress–fracture–seepage solute reaction transport field under different coordinated mining scenarios using a developed multiphysical–chemical model coupled with the FLAC3D-CFD simulator. Finally, the dependence of changes in stratum stress and uranium-bearing solution on the mining technology was analyzed.

2. Coupled Multiphysical–Chemical Field Model

2.1. Modified non-Darcy Flow Model

For high-speed fluids and highly permeable porous media [34], a nonlinear relationship exists between fluid head pressure and non-Darcy flow. Forchheimer's proposed a law in 1901, which has been extensively tested and theoretically verified in the description of the non-Darcy flow [35]:

$$-J = Av + Bv^2 \quad (1)$$

where J is the head pressure gradient, MPa/m; v is the fluid velocity, m/s; A and B are non-Darcy flow factors.

In accordance with previous work [36], the non-Darcy flow factors A and B can be expressed as a function of stress σ , particle diameter D , porosity n , and attribute coefficients $\zeta_1, \zeta_2, \zeta_3, \zeta_4, \zeta_5$, and ζ_6 . These factors are expressed as

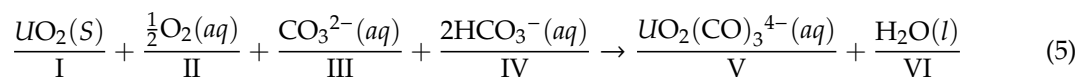
$$v = \frac{2|-J|}{A + \sqrt{A^2 + 4B|-J|}} \tag{2}$$

$$A = \frac{\mu}{k} = a\mu \frac{(1-n)^{\zeta_3}}{n^{\zeta_2}} (1/D)^{\zeta_1} (\sigma)^{-m} \tag{3}$$

$$B = \beta\rho = b_0\rho \exp(c\sigma) \frac{(1-n)^{\zeta_5}}{n^{\zeta_6}} (D)^{-\zeta_4} \tag{4}$$

2.2. Solute Reaction–Transport Model

For alkaline uranium mining, the chemical reaction between natural uranium oxide and leaching solution is described below:



Quality transport of the reactant and producer can be expressed as follows when combined with Equation (5):

$$\partial_t c_{II} + \nabla(c_{II}U) = -\frac{\sigma(c_s)}{\rho\varphi} R_{II} \tag{6}$$

$$\partial_t c_{III} + \nabla(c_{III}U) = -\frac{\sigma(c_s)}{\rho\varphi} R_{III} \tag{7}$$

$$\partial_t c_{IV} + \nabla(c_{IV}U) = -\frac{\sigma(c_s)}{\rho\varphi} R_{IV} \tag{8}$$

$$\partial_t c_V + \nabla(c_VU) = -\frac{\sigma(c_s)}{\rho\varphi} R_V \tag{9}$$

$$\partial_t c_I = -\frac{\sigma(c_s)}{\rho_s(1-\varphi)} R_I \tag{10}$$

where c_I is the uranium oxide grade; c_{II}, c_{III}, c_{IV} , and c_V are the mass solute fractions; U is the transport velocity; $\sigma(c_s)$ is the effective reaction area of the uranium ore; φ is the porosity; R_I is the source of uranium oxide; R_{II}, R_{III}, R_{IV} , and R_V are solute source terms.

Solute transport velocity, which can be directly obtained for the fixed velocity boundary, can also be obtained by the Forchheimer empirical Equation (1) for a constant pressure boundary.

For the transport of a reactive solute, the seepage law in multi-phase can be described as:

$$\frac{\partial \alpha_l \rho_l \phi_l^k}{\partial t} + \nabla \times (\alpha_l \rho_l \vec{u}_l \phi_l^k - \alpha_l \Gamma_l^k \times \nabla \times \phi_l^k) = S_l^k \quad k = 1, \dots, N \tag{11}$$

For a single phase, the volume fraction of al is equal to 1, and Equation (11) can be modified to:

$$\frac{\partial \rho \phi_k}{\partial t} + \frac{\partial}{\partial x_i} \left(\rho u_i \phi_k - \Gamma_k \frac{\partial \phi_k}{\partial x_i} \right) = S_{\phi k} \quad k = 1, \dots, N \tag{12}$$

where ϕ_l^k is the component of the scalar k ; α_l, ρ_l , and u_l are the volume fraction, density, and velocity of the *phase-l*; Γ_l^k, S_l^k are the diffusion coefficient and source item. Under this condition, the scalar of ϕ_l^k is related to the *phase-l* which is considered as an independent zone.

2.3. Multifield Coupled Model

By combining Equations (1) and (3)–(5), we can characterize the response of a mining-induced multiphysical–chemical field:

$$\left\{ \begin{array}{l} UO_2(S) + \frac{1}{2}O_2(aq) + CO_3^{2-}(aq) + 2HCO_3^-(aq) \rightarrow UO_2(CO)_3^{4-}(aq) + H_2O(l) \\ \frac{\partial \rho \varphi_k}{\partial t} + \frac{\partial}{\partial x_i} \left(\rho u_i \varphi_k - \Gamma_k \frac{\partial \varphi_k}{\partial x_i} \right) = S_{\varphi k} \quad k = 1, \dots, N \\ -J = Av + Bv^2 \\ A = \frac{\mu}{k} = a\mu \frac{(1-n)^{\xi_3}}{n^{\xi_2}} (1/D)^{\xi_1} (\sigma)^{-m} \\ B = \beta\rho = b_0\rho \exp(c\sigma) \frac{(1-n)^{\xi_5}}{n^{\xi_6}} (D)^{-\xi_4} \end{array} \right. \quad (13)$$

In accordance with the hydrogeology and mining technology of the mining site, the multifield model (13) can be simplified as follows: (1) The sandstone-type uranium deposit is homogeneous and an isotropic porous medium; (2) The liquid phase is a diluted solution; changes in the liquid density and kinematic viscosity resulting from the chemical reaction were ignored; (3) Changes in porosity caused by the chemical reaction and physical transport were ignored; (4) Solute convection and prominent flow in highly permeable regions of the uranium deposits were located 600 m deep, and the solution diffusion effect was ignored. As a result, constant porosity φ of sandstone-type uranium deposits, uranium density ρ_s , and leaching solution density ρ were assumed during the chemical reaction and physical transport.

3. Coordinate Coal and Uranium Mining

3.1. Mining Geology

The stack area of coal and uranium had a length of 25.49 km, a width of 15.69 km, and a production capacity of 10 million t/a. The 3-1 coal seam was the main coal seam with a depth of 600 m and an average thickness of 3.36 m. For the uranium deposits, the depth was 410 m, and the average thickness was 3.74 m; the distance from the 3-1 coal seam was 90–150 m. The presence of uranium in the lower sandstone area of the Jurassic Zhiluo formation poses a direct threat to the 3-1 coal seam during longwall mining.

3.2. Simulation Setup

The FLAC3D-CFD simulator was used to study the response of the mining deposits while considering coordinate mining scenarios and mining technologies. For the simulation model, the dimension size was 500 m \times 5 m \times 140 m (length \times width \times height), the grid size was 4 m \times 5 m \times 4 m, the space of the pumping well was 30 m, the depth of the coal seam was 600 m, and the overburden stress was 12.07 MPa. The corresponding parameters of the mining technology were: mining length of 320 m, mining speed of 16 m/day, and pumping ratio of injection rate to extraction rate in the range of 1:1–1:4. The hydrogeology condition, specific model and corresponding mechanical and chemical parameters are shown in Figures 1 and 2 and Table 1.

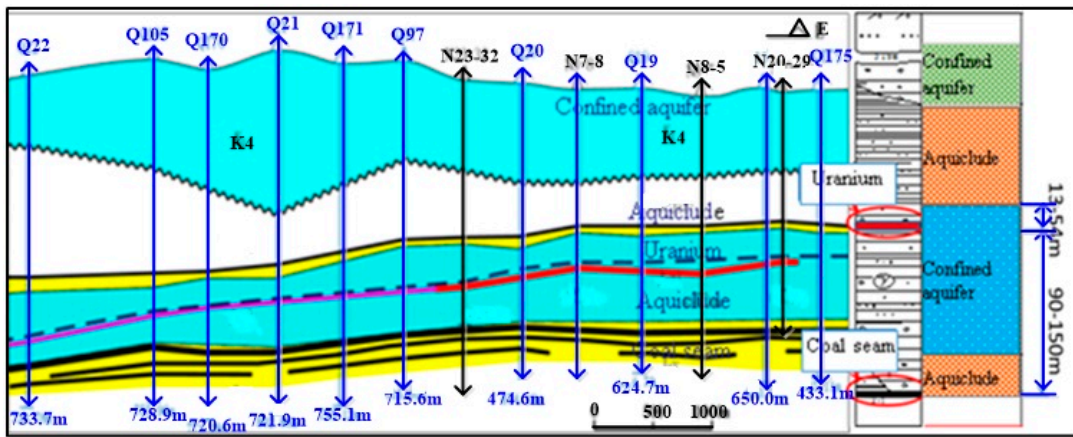


Figure 1. Hydrogeology of the stack resources of coal and uranium.

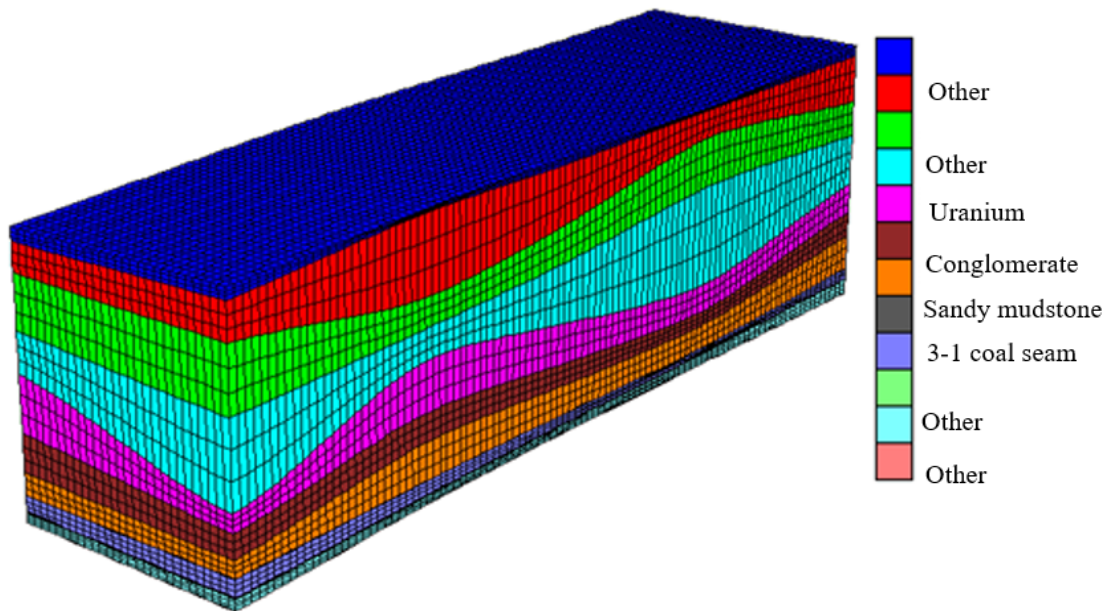


Figure 2. Hydrogeology model.

Table 1. Mechanic and hydraulic parameters for the numerical simulation.

Stress Field	Lithology	Density d (kg/m ³)	Young's Modulus E (GPa)	Poisson's Ratio μ	Cohesion C (MPa)	Strength σ_c (MPa)	Internal Friction ψ (°)	Initial Permeability K (m ²)
	Conglomerate	1800	4×10^{-2}	0.25	8E-3	25	30	-
	Sandy mudstone	2240	15.6	0.30	1.8	27	43	-
	Coal	1600	12.1	0.25	1.1	14	24	-
	Sandy mudstone	2350	13.6	0.32	0.91	50	45	-
Chemical field	Conglomerate	Mass fraction UO_2	Mass fraction O_2	Mass fraction CO_3^{2-}	Mass fraction HCO_3^-	Mass fraction $UO_2(CO_3)_3^{4-}$	Reaction rate (kg/m ³ s)	Diffusion coefficient (m ² /s)
		0.005	0.005	0.01	0.02	0	105/10.5/1.05	-
Seepage field	Conglomerate sandy mudstone	Porosity φ	Initial permeability K (m ²)	Initial non-Darcy coefficient β (m ⁻¹)	Diffusion coefficient (m ² /s)	Longitudinal dispersivity (m)	Transverse dispersivity (m)	-
		0.285	7.0×10^{-12}	1.0×10^8	5×10^{-5}	20	0.67	-

4. Evolution Characteristics of the Multifield Coupling

The mining and environmental occurrence of coal and uranium was reversed by setting the injection and extraction rates for the leaching solute to 9 and 9.27 m³/day, respectively. The hydraulic gradient was set to 0.0013, and the head pressure was set to 3.3–4.3 MPa, according to a previous study [37].

Figure 3 shows that as mining progressed, a negative “pressure funnel” was observed in the overburdened conglomerate, resulting in groundwater inrush in the mining face. Moreover, initiation, propagation, and coalescence of a mining-induced fracture gradually occurred in the surrounding rock. The maximum fracture height of 90 m was obtained as mining progressed to 160 m, and the arch fracture field ripened as mining advanced to 320 m. For the stress field evolution, a skewback was observed in the virgin rock and coal. The stress shell ripened as mining advanced to 130 m and propagated into the stope margins. When mining advanced to 300 m, stress shell rupture occurred, and a new stress shell was generated as a rear skewback was formed by the concentrated stress of the stope. The fluid flow presented a “funnel shape” in the mining face. As a result of the increase in seepage channels and area, the corresponding flow rate increased from 5.0 × 10^{−5} m/s to 7.7 × 10^{−5} m/s as mining advanced. Coal mining induced changes in the stress, seepage, and fracture fields, the mined uranium was dissolved in the solute, and the mixture was transported into the seepage field.

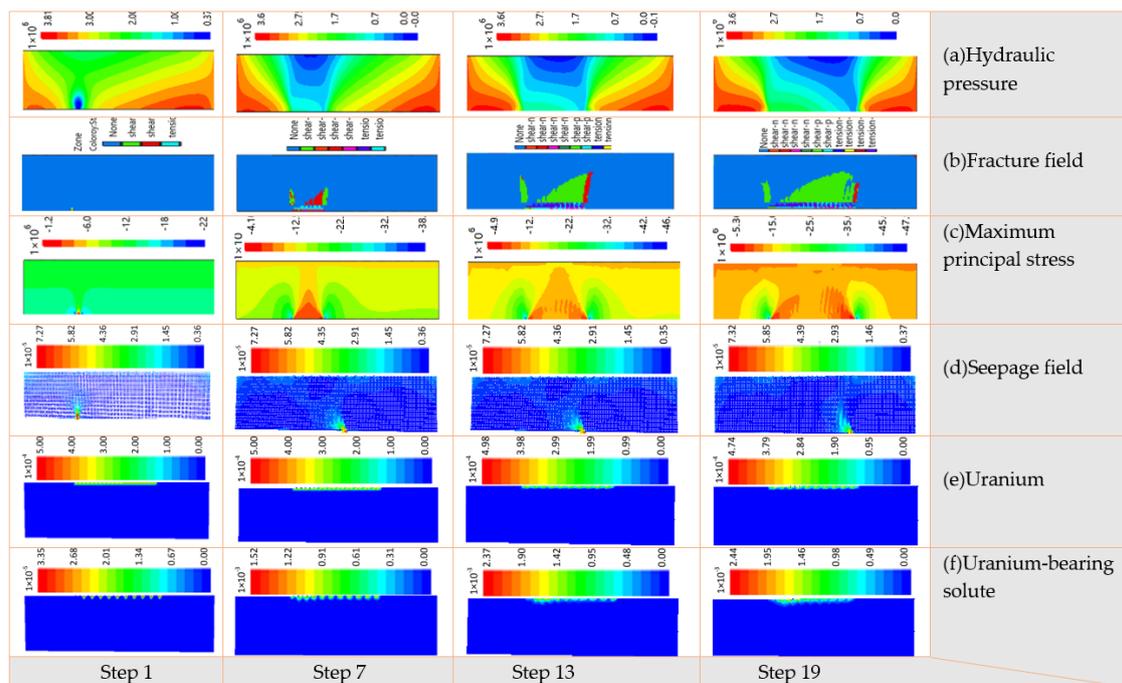


Figure 3. Multifield coupling evolution in the scenario of concurrent coal and uranium mining. (a) Hydraulic pressure; (b) Fracture field; (c) Maximum principal stress; (d) Seepage field; (e) Uranium, (f) Uranium-bearing solute.

As shown in Figure 4, stress concentration and release were obtained, and a decreasing trend was observed with the increase in the distance from the coal seam. Initial stress was recovered at a distance of 120 m behind the mining face as mining advanced to 250 m. For the conglomerate aquifer, a release zone characterized by a “funnel shape” was observed, which propagated into the virgin zones as mining advanced to 250 m. As mining advanced from 250 m to 320 m, the size of the “funnel-shaped” zone reduced progressively, accompanied by the recovery of in situ stress. For uranium deposits, the vertical stress morphology was characterized by a “concave shape”, and stress concentrated at the tip of the concavity. As a whole, the entire stress variation was minor.

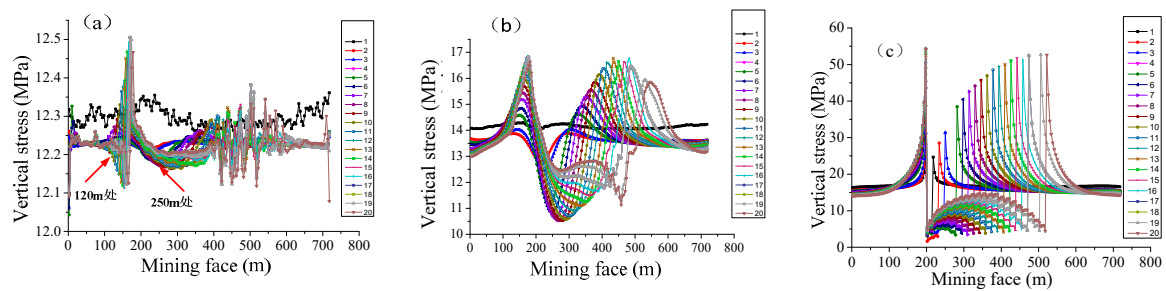


Figure 4. Stress response in the overburden. (a) Redistributed stress in the uranium deposit; (b) Redistributed stress in the conglomerate aquifer; (c) Redistributed stress in the coal seam.

Figure 5 indicates that the concentration of the leaching solution remained stable along the horizontal uranium-bearing deposits. By contrast, the distribution of the uranium-bearing solution was characterized by a “trapezium shape”, and the solution was concentrated at the two ends of the uranium layer. This phenomenon resulted from the hydraulic gradient and the distribution of the pumping well. Under the complex influence of the hydraulic gradient, pumping rate, and diffusion properties, the diffusion depth of the uranium-bearing solution increased at an initial constant rate of 0.12 m/day, which then decreased after 10 days. Finally, the maximum diffusion depth was 5.6 m below the uranium layer.

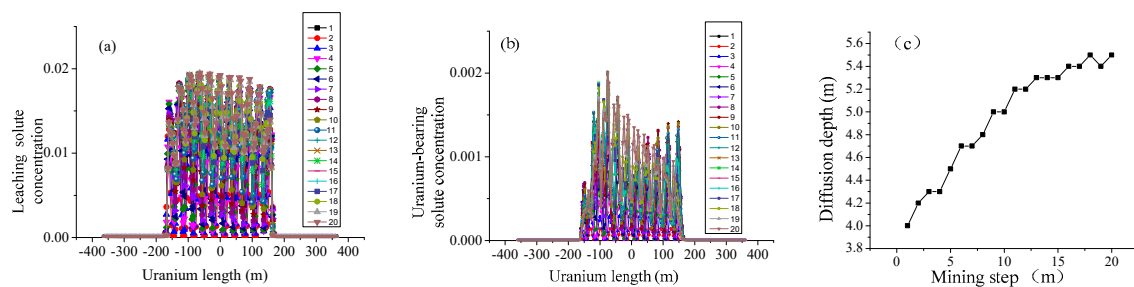


Figure 5. Reactive solute transport and distribution. (a) Distribution of the leaching solution; (b) Distribution of the uranium-bearing solution; (c) Uranium-bearing solution transport.

5. Sensitivity Analysis of the Multifield Coupling

5.1. Effect of the Mining Sequence

5.1.1. Mining of Uranium Prior to Coal

Figure 6 shows the coordinate mining of coal and uranium starting from for uranium. In detail, the hydraulic gradient was set to 0.0013, the concentration of UO_2 , O_2 , CO_3^{2-} , HCO_3^- , and $UO_2(CO_3)_3^{4-}$ reached 0.0005, 0.005, 0.01, and 0.02, respectively. The chemical reaction rate was $k = 10.1$, the diffusion coefficient was 1×10^{-6} , and the injection and extraction rates were 19 and $76 \text{ m}^3/\text{day}$, respectively.

For stope ventilation, a “negative funnel” was developed under the combined effect of the goaf and the confined aquifers characterized by a hydraulic gradient of 7%. As a result, groundwater flowed into the goaf at a rate of $1 \times 10^{-5} \text{ m/s}$. The seepage field was represented by an “inverted funnel” with high permeability at the edge and low permeability in the center, which resulted from the seal effect of the high overburdened stress located at the center of the stope characterized by reduced seepage channels. Meanwhile, the leaching solution was seeped into the stope with a “funnel shape”, which was located directly on the roof of the coal seam. This seeping resulted from the convection diffusion effect of the solute-bearing flow. By contrast, the leaching solution, including the margin and central “funnel-shaped” flows, was characterized by a “W shape” when distributed in the roof and surrounding rock. Finally, the coal stope was filled with the uranium-bearing solution by diffusion over a long period. For mining face ventilation, the difference in hydraulic pressure between the mining

face and the conglomerate-confined aquifer, characterized by a flow rate of 6.13×10^{-5} m/s, resulted in the uranium-bearing solution seeping into the stope with a “semi-saddle shape”. By contrast, the uranium-bearing solution seeped into the stope and mining face with an “asymmetric saddle” morphology under the combined influence of hydraulic pressure and anisotropic permeability of the mining deposits.

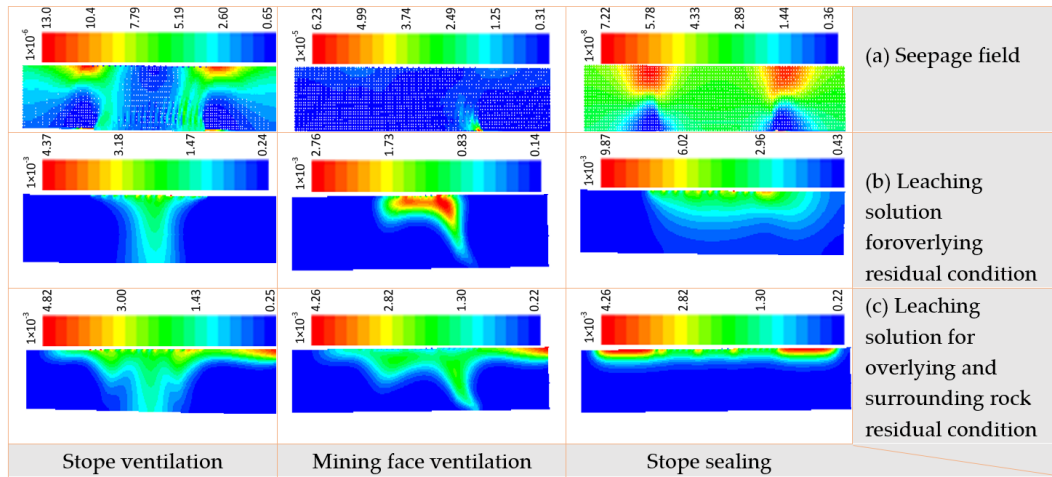


Figure 6. Multifield coupling evolution in the mining of uranium prior to coal. (a) Seepage field; (b) Leaching solution for the overlying residual condition; (c) Leaching solution for the overlying and surrounding rock residual conditions.

5.1.2. Mining of Coal Prior to Uranium

In the scenario of coal mining prior to uranium, the ratio of injection rate to extraction rate was set to 1:1.5, the diffusion coefficient was 1×10^{-5} , the injection rate was $19 \text{ m}^3/\text{day}$, and the reaction rate was 10.5. The evolution and morphology of the seepage–solute reaction transport field is presented in Figure 7.

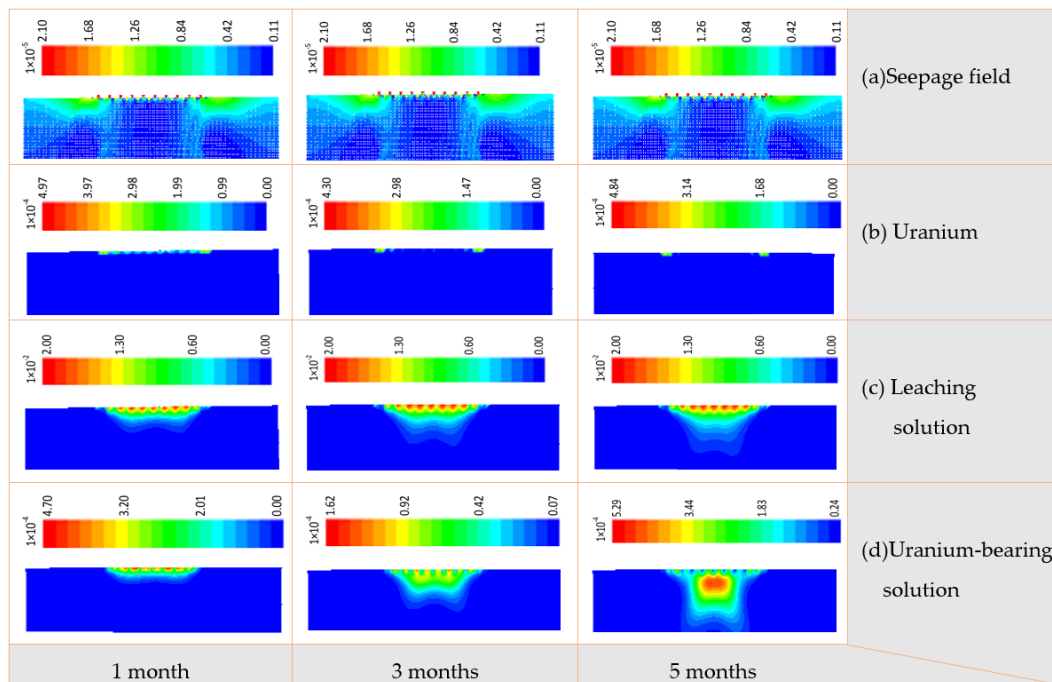


Figure 7. Multifield coupling evolution in stope ventilation. (a) Seepage field; (b) Uranium; (c) Leaching solution; (d) Uranium-bearing solution.

As shown in Figure 7, a division zone of the seepage field was present around the stope shoulder and pumping well due to the influence of hydraulic pressure changes and anisotropy permeability induced by the in situ leaching of uranium and longwall mining of coal. Under the complex effect of convection and diffusion of the solute-bearing flow, a vertical diffusion depth of 8 m toward the coal stope was obtained for the uranium-bearing solution after 1 month of in situ leaching. Subsequently, diffusion depths of 40 and 60 m were obtained, and a “saddle-shaped” morphology for the distribution of the uranium-bearing solution was observed after 3 months of uranium mining. Uranium was completely mined after 5 months, and the uranium-bearing solution migrated into the coal stope.

Figure 8 shows that the hydraulic pressure reached 17% due to the coupled effects of the fractured rock, leaching solution pumping, and confined aquifer on mining face ventilation. Under the integrated effect of seepage and diffusion, the leaching solution and uranium-bearing solution gradually flowed into the mining face with an “asymmetric funnel” morphology after 3 months. The seepage scope gradually enlarged in 1–3 months. By contrast, the efficiency of uranium mining was similar in stope and mining face ventilation.

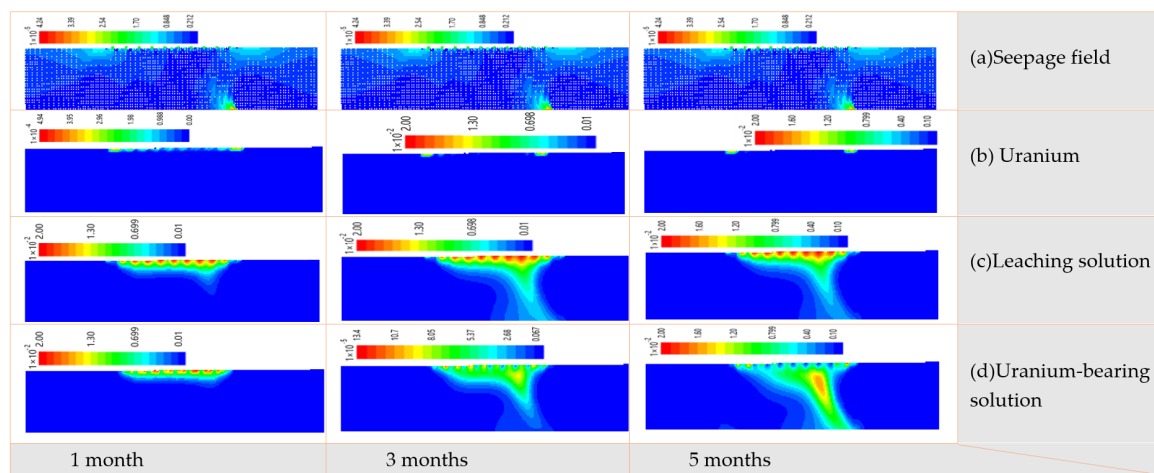


Figure 8. Multifield coupling evolution in the mining face ventilation. (a) Seepage field; (b) Uranium; (c) Leaching solution; (d) Uranium-bearing solution.

5.2. Effect of the Mining Technology

The diffusion scope of the leaching solution is crucial to the safety of coal mining and underground water and considerably related to the injection rate, diffusion coefficient of O_2 , CO_3^{2-} , HCO_3^- and $UO_2(CO_3)_3^{4-}$, and pumping ratio between injection and extraction. To investigate the effect of the injection rate, diffusion parameters, and pumping ratio on the development of the diffusion scope, we set the corresponding parameters as follows: For the first group, the pumping ratio of injection to extraction was 1:1.003 with an injection rate of 19, 25, 30, and 40 m^3/day . The corresponding diffusion coefficients were 0, 1×10^{-5} , 1×10^{-4} , and $1 \times 10^{-3} m^2/s$; For the second group, the pumping ratio of injection to extraction was set to 1:1, 1:2, 1:3, and 1:4 with an injection rate of 19 m^3/day .

As shown in Figure 9a, the diffusion depth was exponentially related to the injection rate and gradually reduced as the injection rate increased. An apparent decrease was obtained at 19–30 m^3/day . Figure 9b indicates that the diffusion depth was positively correlated with the diffusion coefficient and dominated by the seepage velocity when the diffusion coefficient was equal to zero. As the diffusion coefficient increased, the effects of diffusion and mass were promoted, and that of seepage was weakened. In detail, a diffusion depth of 5 m was obtained for the diffusion coefficient of $1 \times 10^{-5} m^2/s$. As the diffusion coefficient increased to 1×10^{-4} and $1 \times 10^{-3} m^2/s$, diffusion depths of 10 and 140 m were obtained, the whole process was dominated by the mass effect, and the seepage effect could be ignored. Meanwhile, the diffusion depth was negatively related to the pumping ratio of extraction to injection, as described in Figure 9. In detail, a diffusion depth of 95 m was obtained

with a pumping ratio of 1:1, and the diffusion depth increased to 10 m for a pumping ratio of 1:2. The maximum diffusion depth was maintained at 4 m with a pumping ratio in the range of 1:2–1:4.

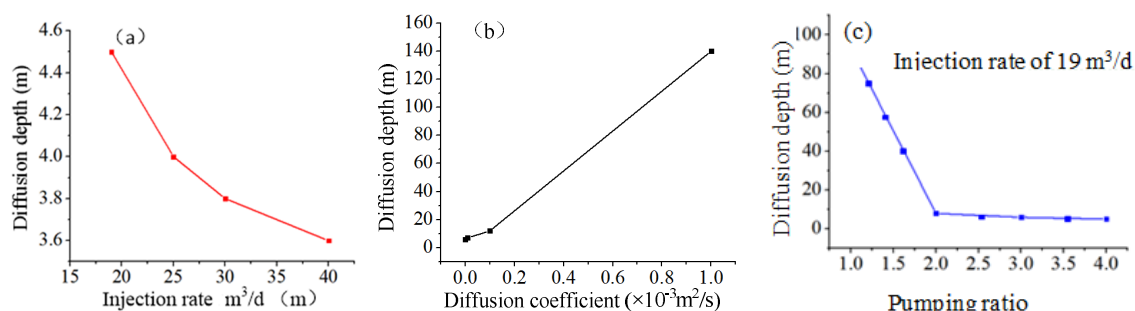


Figure 9. Effect of the mining technology on the development of the uranium-bearing solution. (a) Relationship between injection rate and diffusion depth; (b) Relationship between diffusion coefficient and diffusion depth; (c) Relationship between pumping ratio and diffusion depth.

6. Discussion

In the previous section, we developed a coupled multiphysical–chemical field model, which couples redistributed stress, fracture propagation, fluid migration, and solute diffusion in fractured porous media. Compared with previous efforts in coupling the hydromechanical and hydrochemical fields, the improvements offered by this work are as follows: (1) the hydrogeological response to the coordinate mining of coal and uranium, considering the coupling effects of the stress–fracture–seepage field, solute chemical reaction, and transport, was obtained; (2) the variations of the morphology of the mining-induced multi-field related to mining sequence, ventilation condition, mining technology, and corresponding critical parameters was analyzed. This study identified a stress shell and its forming mechanism and observed mining-induced differences in stress redistribution in the coal seam, conglomerate aquifer, and uranium deposits. An “arch-shaped” fracture field combined with a “saddle-shaped” seepage field was presented. In the scenario of concurrent mining and asynchronous mining of coal and uranium, “funnel-shaped”, “asymmetric saddle-shaped”, “saddle-shaped”, “inclined funnel-shaped”, and “horizontal” morphologies of the leaching solution were described, considering the ventilation in the stope and mining face. The results of this study contribute to stacked resource exploration and environment protection and provide a valued reference for researchers and engineers in this field.

7. Conclusions

(1) A complete stress shell with a maximum fracture height of 90 m was presented, and the overburden stress was transported through a stress arch into the skewback located in the virgin coal and rock mass, as mining advanced to 160 m. Concentrated stress was generated, and the corresponding scope was enlarged, as mining advanced to 256 m. The stress shell became unstable as mining advanced to 280 m. Simultaneously, a new stress shell was generated as a rear skewback was formed by the concentrated stress of the stope.

(2) The influence of mining on the stress response to the coal seam, conglomerate aquifer, and uranium deposits was presented. A dynamic response occurred in the coal seam, and in situ stress recovery was obtained behind the mining face of 120 m, as mining advanced to 250 m. A release zone, characterized by a “funnel shape”, was identified in the conglomerate aquifer, and it gradually reduced as mining advanced. By contrast, slight variations in vertical stress, characterized by a “concave shape”, were found in uranium deposits.

(3) For the scenario of uranium mining prior to coal mining, the leaching solution migrated into the coal stope with a “funnel” shape and “asymmetric saddle” shape under stope and mining face ventilation, respectively. In the scenario of coal mining prior to uranium mining, the leaching solution seeped into the stope with “saddle-shaped” and “inclined funnel-shaped” morphologies.

In the scenario of concurrent coal and uranium mining, the migration of the leaching solution was limited to a short period, and the seepage disappeared in the sealed stope.

(4) The diffusion depth was exponentially related to the injection rate and the pumping ratio between injection and extraction and it was also positively correlated with the diffusion coefficient. In detail, the diffusion depth sharply increased to 140 m as the diffusion coefficient increased to $1 \times 10^{-4} \text{ m}^2/\text{s}$.

Author Contributions: Conceptualization, T.Z. and L.Y.; Methodology, T.Z.; Software, T.Z.; Investigation, T.Z. and Z.W.; Writing—Original Draft Preparation, T.Z. and Y.L.; Writing—Review & Editing, Y.L.; Project Administration, L.Y. All authors have read and agreed to the published version of the manuscript.

Funding: This research was funded by the National Youth Science Foundation (nos.51904011), Anhui Provincial Natural Science Foundation (nos.1908085QE183), Anhui University Scientific Research Foundation (no.QN2018108).

Acknowledgments: This research was supported by the funding and benefited from the comments of the reviewers. We deeply thanks for all of the contributors during the research.

Conflicts of Interest: The authors declare no conflict of interest.

References

- Xia, T.; Zhou, F.; Wang, X.; Zhang, Y.; Li, Y.; Kang, J.; Liu, J. Controlling factors of symbiotic disaster between coal gas and spontaneous combustion in longwall mining gobs. *Fuel* **2016**, *182*, 886–896. [[CrossRef](#)]
- Liu, W.; Qin, Y. Multi-physics coupling model of coal spontaneous combustion in longwall gob area based on moving coordinates. *Fuel* **2017**, *188*, 553–566. [[CrossRef](#)]
- Taraba, B.; Michalec, Z. Effect of longwall face advance rate on spontaneous heating process in the gob area—CFD modelling. *Fuel* **2011**, *90*, 2790–2797. [[CrossRef](#)]
- Guo, H.; Yuan, L.; Shen, B.; Qu, Q.; Xue, J. Mining-induced strata stress changes, fractures and gas flow dynamics in multi-seam longwall mining. *Int. J. Rock Mech. Min. Sci.* **2012**, *54*, 129–139. [[CrossRef](#)]
- Wang, Q.; Cheng, T.; Wu, Y. Influence of mineral colloids and humic substances on uranium (VI) transport in water-saturated geologic porous media. *J. Contam. Hydrol.* **2014**, *170*, 76–85. [[CrossRef](#)]
- Panfilov, M.; Uralbekov, B.; Burkitbayev, M. Reactive transport in the underground leaching of uranium: Asymptotic analytical solution for multi-reaction model. *Hydrometallurgy* **2016**, *160*, 60–72. [[CrossRef](#)]
- Tan, K.; Li, C.; Liu, J.; Qu, H.; Xia, L.; Hu, Y.; Li, Y. A novel method using a complex surfactant for in-situ leaching of low permeable sandstone uranium deposits. *Hydrometallurgy* **2014**, *150*, 99–106. [[CrossRef](#)]
- Yuan, L.; Zhang, T.; Zhao, Y.X.; Ren, B.; Hao, X.J.; Xu, C. Precise coordinated mining of coal and associated resources: A case of environmental coordinated mining of coal and associated rare metal in Ordos basin. *J. China Univ. Min. Technol.* **2017**, *46*, 449–459.
- Letman, M.M.; Drage, J.; Ryan, A.M.; Lake, C.; Jamieson, R. Development of a leaching procedure to assess the risk of uranium leaching due to construction and demolition waste disposal. *Waste Manag.* **2018**, *78*, 144–150. [[CrossRef](#)]
- Saunders, J.A.; Pivetz, B.E.; Voorhies, N.; Wilkin, R.T. Potential aquifer vulnerability in regions down-gradient from uranium in situ recovery (ISR) sites. *J. Environ. Manag.* **2016**, *183*, 67–83. [[CrossRef](#)] [[PubMed](#)]
- Nguyen, V.H.; Gland, N.; Dautriat, J.; David, C.; Wassermann, J.; Guelard, J. Compaction, permeability evolution and stress path effects in unconsolidated sand and weakly consolidated sandstone. *Int. J. Rock Mech. Min. Sci.* **2014**, *67*, 226–239. [[CrossRef](#)]
- Javadi, M.; Sharifzadeh, M.; Shahriar, K. A new geometrical model for non-linear fluid flow through rough fractures. *J. Hydrol.* **2010**, *389*, 18–30. [[CrossRef](#)]
- Nguyen, V.V.; Pinder, G.F.; Gray, W.G.; Botha, J.F. Numerical simulation of uranium in-situ mining. *Chem. Eng. Sci.* **1983**, *38*, 1855–1862. [[CrossRef](#)]
- Zhang, D.; Fan, G.; Ma, L.; Wang, X. Aquifer protection during longwall mining of shallow coal seams: A case study in the Shendong Coalfield of China. *Int. J. Coal Geol.* **2011**, *86*, 190–196. [[CrossRef](#)]

15. Wei, Y.; Dong, Y.; Zhou, P.; Wang, L. Model for simulating hydromechanical responses in aquifers to induced hydraulic stresses: Laboratory investigation and model validation. *J. Nat. Gas Sci. Eng.* **2016**, *30*, 592–603. [[CrossRef](#)]
16. Qiang, W.; Bin, Z.; Shouqiang, L. Flow-solid coupling simulation method analysis and time identification of lagging water-inrush near mine fault belt. *Chin. J. Rock Mech. Eng.* **2011**, *30*, 93–104.
17. Wu, Q.; Zhu, B.; Li, J.M.; Hong, Y.Q.; Qian, Z.J. Numerical Simulation of Lagging Water-Inrush Mechanism of Rock Roadways Near Fault Zone. *J. China Univ. Min. Technol.* **2008**, *37*, 780–785.
18. Weitao, L.; Jianjun, S.; Lianfu, W. Numerical simulation on lag water-bursting at fault zone based on FLAC3D. *J. Liaoning Tech. Univ.* **2012**, *31*, 646–649.
19. Yang, T.H.; Liu, J.; Zhu, W.C.; Elsworth, D.; Tham, L.G.; Tang, C.A. A coupled flow-stress-damage model for groundwater outbursts from an underlying aquifer into mining excavations. *Int. J. Rock Mech. Min. Sci.* **2007**, *44*, 87–97. [[CrossRef](#)]
20. Chen, H.; Zhao, Z.; Sun, J. Coupled hydro-mechanical model for fractured rock masses using the discontinuous deformation analysis. *Tunn. Undergr. Space Technol.* **2013**, *38*, 506–516. [[CrossRef](#)]
21. Kim, J.M.; Parizek, R.R.; Elsworth, D. Evaluation of fully-coupled strata deformation and groundwater flow in response to longwall mining. *Int. J. Rock Mech. Min. Sci.* **1997**, *34*, 1187–1199. [[CrossRef](#)]
22. Jialin, X.; Xiaozhen, W.; Wentao, L. Effects of Primary Key Stratum Location on Height of Water Flowing Fracture Zone. *Chin. J. Rock Mech. Eng.* **2009**, *28*, 380–385.
23. Xie, G.X.; Chang, J.C.; Yang, K. Investigations into stress shell characteristics of surrounding rock in fully mechanized top-coal caving face. *Int. J. Rock Mech. Min. Sci.* **2009**, *46*, 172–181. [[CrossRef](#)]
24. Ma, L.Q.; Zhang, D.S.; Liu, Y.D.; Wang, A.; Zhao, Y.F.; Zheng, T.B. Aquifer- protective Mining Technology in Shallow Coal Seam with Thin Bedrock. *J. Hunan Univ. Sci. Technol.* **2008**, *23*, 1–5.
25. Li, T.; Mei, T.; Sun, X.; Lv, Y.; Sheng, J.; Cai, M. A study on a water-inrush incident at Laohutai coalmine. *Int. J. Rock Mech. Min. Sci.* **2013**, *59*, 151–159. [[CrossRef](#)]
26. Dai Huayang, L.M.; Xianying, M. Analysis of the security of mining under the reservoir in Jiulong Coal Mine of Fengfeng mining area. *J. China Coal Soc.* **2014**, *39*, 295–300.
27. Jun-jie, C.; Wen-bing, G.; You-feng, Z. Feasibility Study on Safe Mining under Large-scale Water Bodies. *China Saf. Sci. J.* **2011**, *21*, 57.
28. Lagneau, V.; Van, D.L.J. Operator-splitting-based reactive transport models in strong feedback of porosity change: The contribution of analytical solutions for accuracy validation and estimator improvement. *J. Contam. Hydrol.* **2010**, *112*, 118–129. [[CrossRef](#)]
29. Li, M.; Huang, C.-M.; Zhang, X.-W.; Gao, F.-Y.; Wu, X.-Y.; Fang, Q.; Tan, W.-F.; Zhang, D. Extraction mechanism of depleted uranium exposure by dilute alkali pretreatment combined with acid leaching. *Hydrometallurgy* **2018**, *180*, 201–209. [[CrossRef](#)]
30. Zheng, C.; Wang, P.P. MT3DMS: A Modular Three-Dimensional Multispecies Transport Model for Simulation of Advection, Dispersion, and Chemical Reactions of Contaminants in Groundwater Systems; Documentation and User's Guide. *Ajr Am. J. Roentgenol.* **1999**, *169*, 1196–1197.
31. Simon, R.B.; Thiry, M.; Schmitt, J.M.; Lagneau, V.; Langlais, V.; Bélières, M. Kinetic reactive transport modelling of column tests for uranium In Situ, Recovery (ISR) mining. *Appl. Geochem.* **2014**, *51*, 116–129. [[CrossRef](#)]
32. Dangelmayr, M.A.; Reimus, P.W.; Wasserman, N.L.; Punsal, J.J.; Johnson, R.H.; Clay, J.T.; Stone, J.J. Laboratory column experiments and transport modeling to evaluate retardation of uranium in an aquifer downgradient of a uranium in-situ recovery site. *Appl. Geochem.* **2017**, *80*, 1–3. [[CrossRef](#)]
33. Gómez, P.; Garralón, A.; Buil, B.; Turrero, M.J.; Sánchez, L.; De la Cruz, B. Modeling of geochemical processes related to uranium mobilization in the groundwater of a uranium mine. *Sci. Total Environ.* **2006**, *366*, 295–309. [[CrossRef](#)] [[PubMed](#)]
34. Oda, M. An equivalent continuum model for coupled stress and fluid flow analysis in jointed rock masses. *Water Resour. Res.* **1986**, *22*, 1845–1856. [[CrossRef](#)]
35. Chen, Y.; Zhou, C.; Sheng, Y. Formulation of strain-dependent hydraulic conductivity for a fractured rock mass. *Int. J. Rock Mech. Min. Sci.* **2007**, *44*, 981–996. [[CrossRef](#)]

36. Zhang, T.; Zhao, Y.; Gan, Q.; Yuan, L.; Zhu, G.; Cai, Y.; Cao, B. Experimental Investigation of Forchheimer Coefficients for Non-Darcy Flow in Conglomerate-Confined Aquifer. *Geofluids* **2018**, *2018*, 1–21. [[CrossRef](#)]
37. Serr-yong, Z.; Lei-chang, S. Optimization of Development and Hoisting Program Design in Poplar River Uranium-Beryllium Mine. *Uranium Min. Metall.* **2017**, *36*, 23–26.



© 2020 by the authors. Licensee MDPI, Basel, Switzerland. This article is an open access article distributed under the terms and conditions of the Creative Commons Attribution (CC BY) license (<http://creativecommons.org/licenses/by/4.0/>).